Eur Biophys J (2007) 36:701–709
DOI 10.1007/s00249-007-0164-0

ORIGINAL PAPER

Large size fibrillar bundles of the Alzheimer amyloid β-protein

Rita Carrotta · Jennifer Barthès · Alessandro Longo · Vincenzo Martorana · Mauro Manno · Giuseppe Portale · Pier Luigi San Biagio

Received: 15 January 2007 / Revised: 20 March 2007 / Accepted: 31 March 2007 / Published online: 11 May 2007

Abstract Self-assembly of amyloid β-protein (Aβ) and its deposition into senile plaques are distinctive features of Alzheimer's disease. Aβ forms typical linear aggregates known as amyloid fibrils, with a diameter of a few tens of nanometers and a length spanning from hundreds of nanometers to micrometers. Fibrils eventually assemble into large size clusters and precipitate in vivo in the brain deposits. Here, we study the late stage of aggregation of Aβ(1–40) in vitro at pH 3.1. We characterize the structure of fibrillar aggregates by a combined use of different experimental techniques. Small angle light scattering, heterodyne near field scattering, large angle light scattering, ultra small angle X-ray scattering and small angle X-ray scattering measurements have been performed to highlight the structural features of amyloid bundles over several lengthscales, from nanometers to tens of micrometers. Phase contrast optical microscopy has been used to complement scattering measurements and directly visualize some morphological details. We show that elongated fibrils of Aβ with a diameter of a few nanometers are packed into large size compact bundles having a typical size of tens of micrometers. The linear morphology of fibrils is reflected in the elongated shape of bundles.

Keywords Amyloid fibrils · Alzheimer · Plaques · Light scattering · X-ray scattering

Abbreviations

Aβ	amyloid β-protein
SALS	small angle light scattering
HNFS	heterodyne near field scattering
LALS	large angle light scattering
SAXS	small angle X-ray scattering
USAXS	ultra small angle X-ray scattering

Proceedings of the XVIII Congress of the Italian Society of Pure and Applied Biophysics (SIBPA), Palermo, Sicily, September 2006.

R. Carrotta
Department of Physics and Astronomical Science,
University of Palermo, via Archirafi 36,
90133 Palermo, Italy

J. Barthès · V. Martorana · M. Manno (✉) ·
P. L. San Biagio
Institute of Biophysics at Palermo,
Italian National Research Council,
via U. La Malfa 153, 90146 Palermo, Italy
e-mail: mauro.manno@pa.ibf.cnr.it

A. Longo
Istituto per lo Studio dei Materiali Nanostrutturati (Palermo),
Italian National Research Council,
via U. La Malfa 153, 90146 Palermo, Italy

G. Portale
Dubble, BM26 ESRF, 6 Rue J. Horowitz,
BP 220, 38043 Grenoble Cedex, France

Introduction

Alzheimer's disease is one of the most common causes of dementia in the elderly (Selkoe 1999). A distinctive feature of this pathology is the presence in the brain of extracellular insoluble deposits, such as senile plaques, diffuse plaques and cerebral amyloid angiopathies. The senile, or neuritic, plaques are mainly spherical structures with a central core made from the amyloid β-proteins (Aβ)s (Iwatsubo et al. 1994), which are also present in the more abundant diffuse plaques (Muller-Hill and Beyreuther 1989), or in the amyloid angiopathy (Rensink et al. 2003). Aβs are small peptides of 39–42 residues (Glenner and

Wong 1984), which can assemble into typical linear aggregates known as amyloid fibrils (Hardy and Selkoe 2002). Similar amyloid fibrils made from different proteins or peptides are associated with other neurodegenerative diseases, such as Parkinson and Huntington diseases, and transmissible spongiform encephalopathy (Lansbury 1999; Temussi et al. 2003). The onset of Alzheimer's disease seems to be primarily related to a synaptic dysfunction preceding neuronal degeneration, rather than caused by the amyloid deposits (Terry et al. 1991; Selkoe 2002). However, the production of Aβ, and the presence of amyloid deposits is strictly associated with the disease. The study of the structural properties of such deposits is therefore of great interest to improve the methods for non-invasive diagnosis, which may be available with the recent advances in neuroimaging (Mathis et al. 2005; Small et al. 2006), as well as in the detection of pathological biomarkers (Pitschke et al. 1998; Georganopoulou et al. 2005).

On a molecular lengthscale, Aβ can form a variety of aggregates, which have been observed under different conditions in vitro. These structures include amyloid fibrils (Ban et al. 2004), small toxic oligomers (Walsh et al. 1997; Lambert et al. 1998), spherical amyloid particles (Westlind-Danielsson and Arnerup 2001; Hoshi et al. 2003), annular pore-forming structures (Lashuel et al. 2002), amyloid protofibrils (Harper et al. 1997), beaded chain protofibrils (Huang et al. 2000), spherocylindrical micelles (Lomakin et al. 1996; Yong et al. 2002).

In our previous work (Carrotta et al. 2005), we have studied the mechanism of Aβ(1–40) fibrillation at pH 3.1. We have shown that peptides coexist with oligomers with an average aggregation number of 75 units. Amyloid formation occurs via a non-cooperative coagulation process, which closely resembles linear colloidal aggregation. Interestingly, a single activation free energy barrier has been found to be responsible for the coagulation rate. The study of Aβ(oligomers and of their fibrillation is particularly important since they have been shown to be highly toxic for embryo development (Carrotta et al. 2006), and for neuronal activity (Walsh et al. 2002).

In the present work, we study the late stages of Aβ(1–40) aggregation at acid pH. Fibrils formed from Aβ oligomers at low pH have the same characteristics as fibrils formed at physiological pH (Lomakin et al. 1996) and a high experimental reliability (Carrotta et al. 2005). Therefore, although acid pH is not a physiological condition for amyloid deposition, it is of high interest in order to address the Aβ self-organization at the molecular level and to highlight a fibrillation process which initiates from Aβ oligomers. The morphological properties of aggregates have been studied by phase contrast microscopy and by several scattering techniques: Small angle light scattering (SALS), heterodyne near field [light] scattering (HNFS), large angle light scattering (LALS), ultra small angle X-ray scattering (USAXS) and small angle X-ray scattering (SAXS). The combined usage of these techniques allows one to observe the structural features of amyloid aggregates over several lengthscales, from nanometers to tens of micrometers.

Microscopy images show large-size aggregates, with an elongated shape, and suggest that they are built by smaller filamentous objects, resembling amyloid fibrils. The complex structure suggested by these observations has been used as a guide for the analysis of scattering data. The aggregate form factor, obtained by matching all scattering data, has been analysed by a model of hierarchical form factors, which encompasses the aggregate morphologies over all the lengthscales.

In summary, we observed that the elongated amyloid structures, which form in the early stages (Carrotta et al. 2005), coalesce into larger bundles of fibrils. These bundles are rather compact aggregates, with a typical size of tens of micrometers. They are made from cylindrical elongated objects with a typical length of hundred of nanometers, and a diameter of about 8 nm.

Here, we are addressing amyloid morphology in one important particular case, among the variety of structures, which originates from Aβ aggregation. The wide range of lengthscales covered in this work (five orders of magnitude) is challenging to extend these morphological studies to other conditions and to correlate these structures with the brain deposits such as senile plaques and amyloid angiopathy.

Materials and methods

Sample preparation

All chemicals used for preparation of the amyloid β-protein solutions were of analytical grade. Aβ(1–40) peptide (purchased from Anaspec) was pre-treated with trifluoroacetic acid as described in a previous work (Carrotta et al. 2005). Peptide solutions were prepared by dissolving in 0.1 M Na-citrate buffer at pH 3.1 the peptide powder obtained from the trifluoroacetic acid treatment. The solution was filtered with a 0.2-μm Millex-LG filter into quartz cuvettes or glass vials for incubation at the desired temperature. Peptide concentration was 185 μM, i.e. 0.8 mg/ml. The concentration was determined by measuring tyrosine absorbance at 276 nm (ε_{276} = 1,390 M^{-1} cm^{-1}), with a Jasco J-530 spectrophotometer.

Photon correlation spectroscopy

The aggregation process of the amyloid β-protein was monitored by photon correlation spectroscopy, which

provides the intensity autocorrelation function. The sample was held in a thermostated bath at $T = 37°C$ and moved for the measure to a thermostated cell compartment of a Brookhaven Instruments BI-200-SM goniometer, equipped with a 100 mW Ar laser, tuned at $l_0 = 514.5$ nm. Temperature was controlled within 0.05°C. A Brookhaven BI-9000 correlator was used to measure simultaneously scattered light intensity at 90° and its autocorrelation function, $g_2(t)$. Autocorrelation functions were analysed by using a constrained regularization method (Stepanek 1993), according to the expression $g_2(t) = 1 + \beta^2 | \int P(D) \exp(-Dq^2 t)\, dD |^2$, where $P(D)$ is the distribution of the apparent diffusion coefficients D, β is an instrumental factor, q is the scattering vector $q = 4\pi n_0 \lambda_0 \sin(\vartheta/2)$, with ϑ the observation angle and n_0 the medium refractive index. The z-averaged hydrodynamic radius R_h has been calculated from the apparent diffusion coefficient D by assuming the Stokes–Einstein relation: $k_B T D^{-1} = 6\pi\eta R_h$, where k_B is the Boltzmann constant, T the temperature and h the solvent viscosity (Berne and Pecora 1976).

Large angle light scattering

The experimental set up and procedure described for photon correlation spectroscopy experiments was also used for LALS measurements. Multiple angle experiments were performed in order to determine the scattered intensity $I(q)$ at different scattering vectors, covering a range of q from 5 to 30 μm^{-1}. The scattered intensity $I(q)$ is given in terms of Rayleigh ratio $R(q) = I(q) / I_0 r^2 / V_s$, where I_0 is the intensity of the laser source, V_s is the scattering volume, and r is the distance of the detector from the sample. Absolute values for scattered intensity (Rayleigh ratio R) have been obtained by normalization with respect to toluene, whose Rayleigh ratio was taken as 32×10^{-6} cm^{-1} at $\lambda_0 = 514.5$ nm.

Small angle light scattering

An SALS experiment has been performed on a sample incubated for 70 days at $T = 37°C$, obtained by using the same sample preparation which has been used for LALS experiments. The experiment was performed by using an experimental device built in our laboratory (Bulone et al. 2004; Manno et al. 2006), and equipped with a 30 mW Melles Griot helium–neon laser and a charge coupled device Pulnix TM765 camera. Measurable intensities span a wide dynamical range (from 1.0 to 33105, in arbitrary units), thanks to a software integration of multiple exposure times (1/60–1/10,000 s). After background subtraction (performed by home-made software), reliable measurements could be made over a range of scattering angles of 0.1°–11° (with a maximum resolution of 0.01°), corresponding to scattering vector magnitudes of 0.02–2 μm^{-1}.

Heterodyne near field scattering

Heterodyne near field [Light] scattering experiments have been performed on a 185 μM Aβ(1–40) solution incubated at $T = 37°C$.

The HNFS is a self-referencing method, in which the static intense transmitted beam acts as a local oscillator that amplifies the weak fluctuating scattering signal, leading to a direct measurement of the scattered field amplitude. With this innovative technique, the optical setup is really simple and does not require an accurate alignment. Furthermore, HNFS allows one, in principle, to access a larger range of scattering angles with respect to the traditional SALS, and it does not require a separate measurement of the stray light pattern (Ferri et al. 2004). The technique is based on the property that the speckles of the scattered field $f(\mathbf{r},t)$ (where $\mathbf{r}$ is a vector lying on a plane perpendicular to the illuminating beam), measured close enough to the sample, are of the same size of the scatterers. The presence of the transmitted beam contributes a static background that must be subtracted in order to recover the fluctuating scattered field. The subtraction is accomplished by calculating the difference $\delta f(\mathbf{r},t,\Delta t)$ between two frames spaced by a time interval Δt. A Fourier transform is then required to obtain the scattered intensity versus the wave vector q (Ferri et al. 2004): $I_s(q) = \langle |FT\{(\delta f(\mathbf{r},t,\Delta t)\}|^2 \rangle_{t,|\mathbf{q}|=q}$ where the averages are over the measurement time and the azimuthal angle of the wave vector.

The apparatus comprises an He–Ne laser (JDS Uniphase He-Ne Gas laser 1135P) of wavelength $\lambda_0 = 632.8$ nm whose beam is spatially filtered and expanded. This large collimated beam of diameter $D = 16$ mm illuminates the sample contained in a circular quartz cell with a 2 mm optical path. The heterodyne signal, due to the interference between the transmitted and the scattered light, is collected by a microscope objective (Edmund Optics 20×, NA = 0.4). The objective relays onto the camera sensor plane (PixeLink CMOS PLA741 1,280 × 1024 pixels, pixel pitch 6.7 mm, 10 bit) a magnified image of a plane located at distance $z = 9$ mm from the cell. The theoretical accessible range of scattering angles is determined by the objective numerical aperture and magnification for the upper limit (~ 4 μm^{-1}), and by the sensor size for the lower limit (~ 0.022 μm^{-1}). The images, acquired at the rate of 1 Hz, are analysed after the completion of data acquisition by home-made software. The choice of Δt is a crucial point in analysing these data. In order to assign contributions from the largest (very slow) aggregates in the fluctuating signal, Δt should be set as large as possible. On the other hand, we observed that low q intensities were heavily affected by the

presence of slow mechanical instabilities of the apparatus, which come into play when large Δt are used. Consistent results were obtained by using $\Delta t = 1$ s for all the samples, except for the one held for 70 days at $T = 37$°C. In this case, we increased the Δt value to 5 s to avoid the dampening of the scattered field of slowly diffusing, larger aggregates. Further, we had to restrict the valid q range to the interval 1.5–3 μm^{-1}.

Small and ultra-small angle X-ray scattering

X-ray scattering experiments have been performed on a 185 μM Aβ(1–40) solution incubated at $T = 67$°C for 2 h.

X-ray measurements were performed at the synchrotron DOUBLE beamline BM26B at the European Synchrotron Radiation Facilities (ESRF, Grenoble, France; Borsboom et al. 1998). Experiments were carried out using a monochromatic 12 keV X-ray beam. The H-hutch of BM26 is equipped to perform SAXS, USAXS, as well as Wide Angle X-ray Scattering (WAXS) experiments. It was designed with a maximum of flexibility that allows one to study several problems, particularly in the field of polymer science (Bras 1998). In our experiments, the small and ultra-small angle scattering images were recorded by placing a two-dimensional position sensitive detector at two different sample-to-detector distances, respectively, 1.5 and 8 m. Thus, a large scattering vector range was covered (5×10^{-3}–0.35 $Å^{-1}$). In order to obtain the isotropic USAXS/SAXS intensity profiles, the two-dimensional images were radially averaged around the centre of the primary beam using FIT2D software (Hammersley 1997). Silver Behenate (for the 1.5 m sample-detector distance) and rat tail tendon collagen (for the 8 m sample-detector distance) were used as standards to determine the centre of the beam and the scattering vector scale. Before joining the two partial profiles recorded with the two different sample-detector distances, the scattering from the empty cell was subtracted from the raw data. In order to do this, each spectrum was at first normalized for the intensity of the incident beam; then the scattering from the empty cell was subtracted after correction for transmission difference between the sample and the empty cell. Such difference has a certain experimental error, due to the small gap between the electronic density of the sample and that of the empty cell. The quality of the data is obviously affected by this uncertainty at low scattering vectors. At the end, the two corrected curves were successfully superimposed with a good overlap range (0.03–0.06 $Å^{-1}$).

Optical microscopy

At the end of scattering experiments (after 13 days of incubation at 37°C and 47 days at room temperature), a few drops of solution were put on a glass for imaging with a phase-contrast Zeiss Axioskop2 plus microscope.

Results and discussion

Late stage of aggregation

The late stage of the aggregation process of the amyloid β-protein (1–40) has been studied from 4 h to 70 days at pH 3.1, 37°C, and 185 μM. This is a follow-up of our previous work (Carrotta et al. 2005), where we studied the early stages of aggregation kinetics. Under the present experimental conditions, large-mass oligomers made from about 75 peptides are present in the solution since the very beginning (consistent with other findings under similar conditions by Lomakin et al. (1996)). In the early stages, the amyloid fibrillation proceeds via diffusion and coagulation of clusters of different sizes, which assemble into flexible elongated polymers. It is noteworthy that the same process operates at different temperatures (at least in the range 27–67°C) and that the coagulation is controlled by a single free energy barrier (Carrotta et al. 2005).

In the present work, we extend the duration of kinetics up to 70 days. By photon correlation spectroscopy we measure the correlation of the scattered light intensity at a scattering vector $q = 23$ μm^{-1} and analyse the data by using a regularization method with a smoothing constraint, which yields the distributions of the z-averaged hydrodynamic radii. The size distributions at four representative times are reported in Fig. 1. After 4 h of incubation at 37°C a broad size distribution shows the presence of species from 10 to 50 nm (Fig. 1a), with an apparent average hydrodynamic radius of about 15 nm, agreeing with our previous work (Carrotta et al. 2005). In 3 and 13 days the average hydrodynamic diameter grows to about 50 and 100 nm, respectively (Fig. 1b, c). This sample was afterwards left at room temperature for 47 days. An interesting broad distribution clearly evidences heterogeneity and the presence of a population of huge objects with a size larger than micrometers. However, the effective population of these large species is strongly underestimated with respect to the other species, due to the effect of their form factor at $q = 23$ μm^{-1}.

In order to perform scattering measurements at long incubation times and to get information about larger size aggregates, we used the HNFS measurements. HNFS is an innovative technique (Ferri et al. 2004), which does not require a separate measurement of the background scattering from the solution. Therefore, it allows one to measure the scattering patterns from a sample over days or months, and to put them on an absolute scale, at least with respect to each other. Figure 2 shows the HNFS measurements at different times of 185 μM Aβ incubated at 37°C.

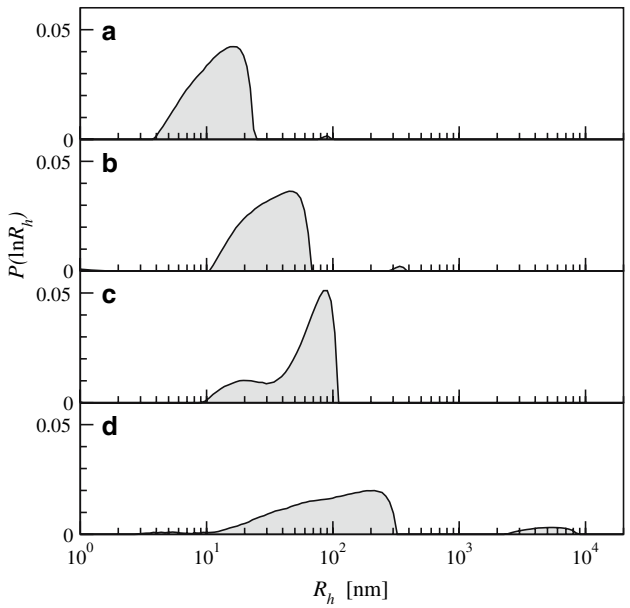

Fig. 1 Distribution function of the hydrodynamic radii at selected times of a 185 μM Aβ solution incubated at 37°C. Times elapsed after incubation: **a** 4 h, **b** 3 days, **c** 13 days. **d** 60 days (namely, 13 days at 37°C and 47 days at room temperature). Data analysis was performed as reported in the text

We observe a monotonic increase of the total intensity over time, while the shape of the structure function has slight changes. This shows that after a few days, the same aggregates of microscopic size are already formed and their number and (likely) their size increase with time.

Structure of amyloid bundles

The morphology of the Aβ aggregates formed after incubation at 37°C has been observed by phase contrast microscopy. Figure 3 displays some typical aggregates. They are elongated aggregates with a size larger than tens of micrometers. The heterogeneity of shapes and sizes is a clear result of a kinetic coagulation process. Their filamentous appearance suggests that they originate from already formed fibrils.

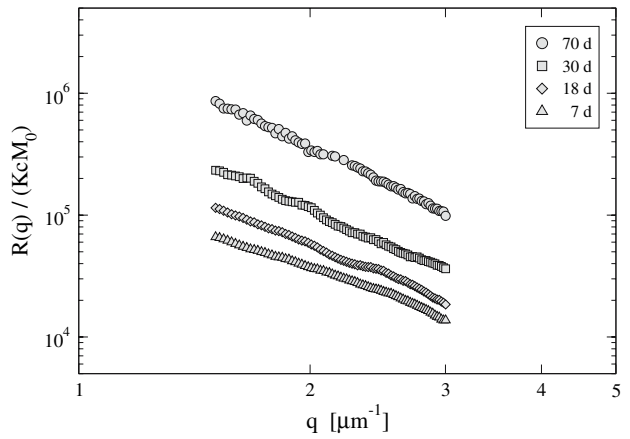

Fig. 2 Heterodyne near field scattering (in terms of normalized Rayleigh ratio) at selected times of a 185 μM Aβ solution incubated at 37°C. Times elapsed after incubation: 7 days (*triangles*), 18 days (*diamond*), 30 days (*squares*), 70 days (*circles*)

In Fig. 3, we note smaller aggregates with a size of a few micrometers. They seem to have a quite spherical shape, but the resolution of the images does not allow us to establish if they have the same morphological features of the larger objects. Also note that the size of the aggregates of Fig. 3 has larger values with respect to the hydrodynamic radii of Fig. 1. This is likely due to the difference in the thermal history of the two samples.

In order to get more quantitative, and statistically significant, information about the structural properties of such aggregates, we used several scattering techniques on the same 185 μM sample incubated for 70 days at 37°C. Figure 4 shows the structure function measured by SALS, HNFS, and LALS. The absolute scale of LALS has been determined by toluene calibration that of SALS and HNFS by matching the shape of scattering profiles with LALS data. In Fig. 4, we observe a power-law dependence in the range of scattering vectors between few micrometers and tens of nanometers. This is typical of aggregates having a radius of gyration r_b of tens of micrometers, consistent with microscopy images, which are made from smaller units with a size r_b of tens of nanometers. The scattering data of Fig. 4 are plotted in terms of the normalized Rayleigh ratio $R(q)\ (KcM_0)^{-1}$, where c and M_0 are respectively the peptide mass concentration and molecular mass, and K is an instrumental factor: $K = 4\pi\tilde{n}^2\ (\mathrm{d}\tilde{n}/\mathrm{d}c)^2\ \lambda_0^{-4}\ N_A^{-1}$, where $\tilde{n}$ is the medium refractive index, λ_0 is the incident wavelength, and N_A is the Avogadro's number (Berne and Pecora 1976). The scattering profile is therefore related to the form factor of the amyloid bundles $P_b(q)$ of mass M_b, and z-averaged aggregation number $n_z = M_b/M_0$:

$$\frac{R(q)}{KcM_0} = n_z P_b(q). \tag{1}$$

We fit the data by using a general function developed to model fractal aggregates with fractal dimension d, radius of gyration r_b and mass M_b, made from smaller objects of size r_f and mass M_f (Nicolai et al. 1996):

$$S_d(q; r_b, r_f) = \frac{1}{n_b}\left[1 + \frac{n_b - 1}{\left[1 + (\xi q)^2\right]^{\frac{d-1}{2}}}\,\frac{\sin\left((d-1)\mathrm{atan}(\xi q)\right)}{(d-1)\,\xi q}\right] \tag{2}$$

where $\xi = r_f/(d(d+1)/2)^{0.5}$ is the correlation length, and $n_b = M_f/M_f$ is the number of units which are assembled in

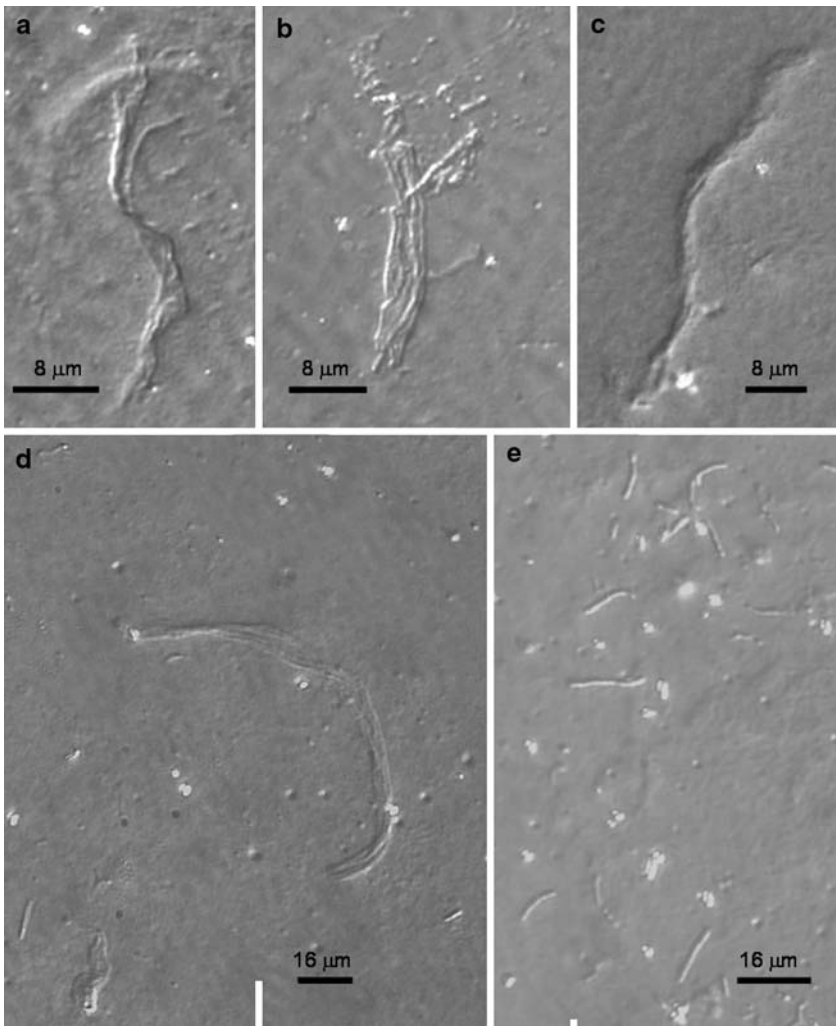

Fig. 3 Phase contrast microscopy images of a 185 μM Aβ solution after incubation for 13 days at 37°C and 47 days more at room temperature

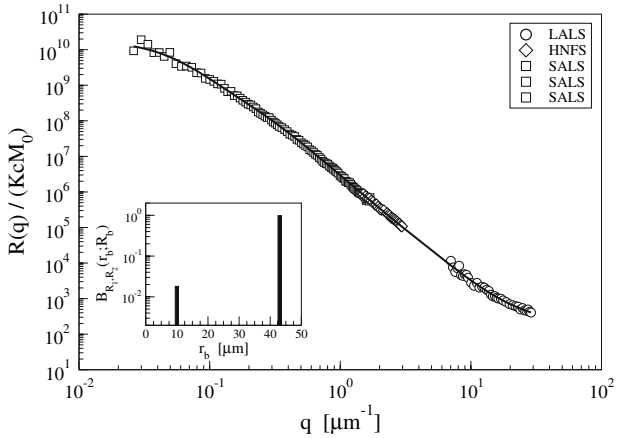

Fig. 4 Scattered intensity (in terms of Rayleigh ratio) of a 185 μM Aβ solution incubated at 37°C for 70 days. Different symbols refer to different techniques: *circles* large angle light scattering (LALS); *diamonds* heterodyne near field scattering (HNFS); *squares* small angle light scattering (SALS). The *line* is the data best fit according to expressions 1–3. In the *inset*: Distribution function $B_{R1;R2}(r_b;R_b)$ of the radii of gyration of the bundles (see expression 2)

one aggregate: $n_b = 1 + \Gamma(d+1)\,(\xi/r_f)^d$, where $\Gamma(x)$ is the Gamma function. Here, we fit the data of Fig. 4 by allowing a polydispersity in the radii of gyration r_b, and by using a bimodal distribution function $B_{R1,R2}(r_b;R_b)$ with average R_b:

$$P_b(q) = \int B_{R1,R2}(r_b;R_b)\; S_d(q;r_b,r_a)\; \mathrm{d}r_b \qquad (3)$$

$$B_{R1,R2}(r_b;R_b) = \frac{R_b - R_2}{R_1 - R_2}\delta(r_b - R_1) + \frac{R_1 - R_b}{R_1 - R_2}\delta(r_b - R_2).$$

By using eqs. 1–3, we obtained the following best-fit parameters: $R_1 = 43$ μm, $R_2 = 10$ μm, $R_b = 42.4$ μm, $r_f = 31.5$ nm, $d = 2.8$, $n_z = 18 \times 10^9$.

Expression 3 is very general. Indeed, it introduces a very minimalistic model for the structure of the aggregates. From this expression, we can obtain only three parameters: the size of aggregates, the size of the constituent units, and the fractal dimension, which is essentially a measure of the

packing of the small units into the large aggregates. In the present case, the value of $d = 2.8$ very close to 3 suggests that aggregates are rather compact objects (Manno et al. 2007). The size of such aggregates is of the order of tens of micrometers, and it is therefore consistent with the objects observed in microscopy images. As we shall see, the characteristic size of the building blocks of such aggregates ($r_f = 31.5$ nm) is consistent with that of amyloid fibrils.

Structure of amyloid fibrils

The structure of the fibrils which eventually assemble into bundles has been studied on a smaller length scale by X-ray scattering. Amyloid fibrils and aggregates have been prepared by incubating a 185 μM Aβ solution at 67°C for 2 h. As shown in our previous work (Carrotta et al. 2005), this is equivalent to an incubation at 37°C for a few days. Afterwards, the sample has been quenched to 5°C and used for both SAXS and USAXS experiments. In Fig. 5, X-ray data are shown together with LALS data obtained after 3 days of incubation at 37°C. The X-ray intensity is scaled accordingly to the absolute scale of LALS data, although there is a gap between LALS and USAXS data. The scattering profile is related to the form factor of the amyloid fibrils $P_f(q)$ of mass M_f, and z-averaged aggregation number $n_f = M_f/M_0$:

$$\frac{R(q)}{KcM_0} = n_f P_f(q). \tag{4}$$

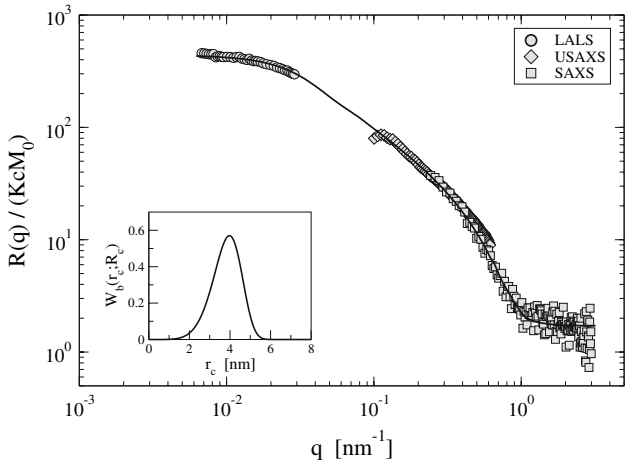

Fig. 5 Scattered intensity (in terms of normalized Rayleigh ratio) of a 185 μM Aβ solution incubated at 67°C for 2 h (X-ray data) or at 37°C for 3 days (LALS data). Different symbols refer to different techniques: *circles* large angle light scattering (LALS); *diamonds* ultra-small angle X-ray scattering (USAXS); *squares* small angle X-ray scattering (SAXS). The *line* is the data best fit according to expressions 4–6. In the *inset*: Distribution function $W_b(r_c;R_c)$ of the radii of *cylinder* (see expression 6)

The data can be fit by using the form factor of a cylinder of radius r_c, and height h_c (Pedersen 1997):

$$P_c(q;r_c,h_c) = \int_0^{\pi/2} \left[\frac{2j_1(qr_c\sin\alpha)}{qr_c\sin\alpha} j_0\left(\frac{1}{2}qh_c\cos\alpha\right)\right]^2 \sin\alpha\, d\alpha \tag{5}$$

where j_0 and j_1 are respectively the spherical Bessel function of first kind of order 0 and 1: $j_0(x) = \sin(x)/x$, $j_1(x) = \sin(x)/x^2 - \cos(x)/x$. As for light scattering data, we fit the data of Fig. 5 by allowing a polydispersity in the radius r_c of the cylinder, and by using a Weibull distribution function $W_b(r_c;R_c)$ with average R_c (Pedersen 1993). Also, we add a baseline B to take into account the molecular details on the Ångström lengthscale, which are not resolved by our data.

$$P_f(q) = \frac{9}{4}(1-B)\int W_b(r_c;R_c)\, P_c(q;r_c,h_c)\, dr_c + B \tag{6}$$

$$W_b(r_c;R_c) = b\left[\frac{\Gamma\left(\frac{1}{b}+1\right)}{R_c}\right]^b r_c^{b-1} \exp\left(-\left[\frac{r_c\,\Gamma\left(\frac{1}{b}+1\right)}{R_c}\right]^b\right).$$

The fit does not take into account the decrease of the structure function at low scattering vectors, which is an artefact due to a not perfect background subtraction.

By using Eqs. 4–6, we obtained the following best-fit parameters: $R_c = 3.8$ nm, $h_c = 133$ nm, $b = 6.25$, $B = 0.0045$, $n_f = 440$. For a rigid cylinder the radius of gyration r_g is related to the height and radius, through the relation: $r_g^2 = h_c^2/12 + R_c^2/2$. Thus, we obtain $r_g = 38.5$ nm.

The parameter b is a measure of radii polydispersity. Equivalently, it may be read as an effect of a cylindrical eccentricity. Indeed, a fit of comparable quality is obtained by using the form factor of a rigid cylinder with an elliptical cross section (data not shown). Interestingly, the values of the axes obtained from the fitting (5 and 13 nm) are consistent with the size of the spherocylindrical micelles observed on Aβ(1–40) under similar conditions by Yong et al. (2002).

Structure of amyloid bundles of fibrils

The range of scattering vectors in the *X*-ray measurements is focused on the nanometer scale. Thus, we can study the structure of amyloid fibrils without considering if they are free in solution or already assembled into bundles. Indeed, the parameters obtained by fitting the data of Fig. 5 are really reliable only when related to the nanometer scale. In particular, the radius R_c is well determined by the change in the slope of X-ray scattering data, while the

height h_c and the aggregation number n_f are less robust parameters, since they are obtained by matching LALS and SAXS data.

With this warning, we try now to match the light scattering data of Fig. 4, obtained upon incubation at 37°C for 70 days, with the X-ray scattering data of Fig. 5. As we just remarked, this is reasonable, since the structural properties of the aggregates larger than nanometers are transparent to X-ray. On the other hand, the structural details on the nanometer scale are not resolved by light scattering data. In Fig. 6, we show the data obtained by all the scattering techniques. The data can be fit by assuming a model of hierarchical form factors (Pedersen 1997; Manno et al. 2007). We first calculate the form factor of amyloid fibrils $P_f(q)$, and then we calculate the form factor of amyloid bundles assuming that their constituent units are the fibrils itself. The overall form factor of aggregates is obtained by the product of the two form factors. Data are fit by expression:

$$\frac{R(q)}{KcM_0} = n_b P_b(q)\, n_f P_f(q) \tag{7}$$

where the symbols have the same meaning defined above in the text and in expressions 2, 3, 5, and 6. The best-fit parameters have the same values of previous fitting, except of course for the fibril aggregation number n_f and the fibril height h_c, for the reasons discussed above. In the present case, we have $n_f = n_z/n_b = 142$ and $h_c = 109$ nm, which corresponds to a radius of gyration $r_g = 31.5$ nm This value is equivalent to the size of the building block of the bundles ($r_g = r_f$), as seen in expressions 1–3. Actually, the same parameter was used for fitting.

It is remarkable that the X-ray scattering data may be matched with light scattering data collected both after 3 days and after 70 days of incubation. In other words, the same cylindrical morphology observed on the nanometer lengthscale can be fit in the structure of freely diffusing fibrils (Fig. 5), as well as in the more complex and larger structure of fibrillar bundles (Fig. 6).

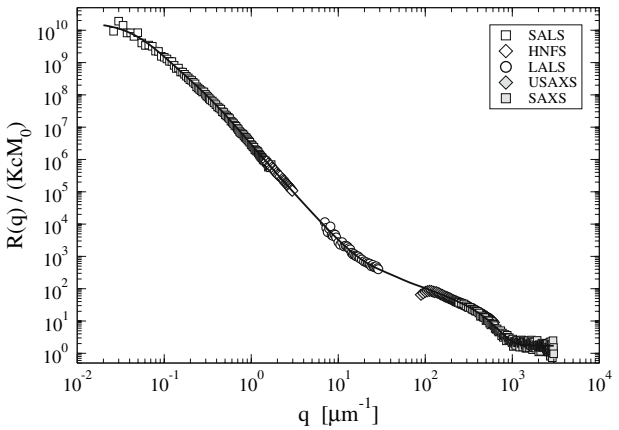

Fig. 6 Scattered intensity (in terms of normalized Rayleigh ratio) of a 185 μM Aβ solution incubated at 67°C for 2 h (X-ray data) or at 37°C for 70 days (*light data*). Different symbols refer to different techniques: *white circles*, *large angle light scattering* (SALS); *white diamonds* heterodyne near field scattering (HNFS); *white circles* large angle light scattering (LALS); *grey diamonds* ultra-small angle X-ray scattering (USAXS); *grey squares* small angle X-ray scattering (SAXS). The *line* is the data best fit according to expressions 2, 3, 5–7

Conclusions

In the present work, we have studied the supramolecular aggregates of the amyloid β-protein (1–40), which is related to Alzheimer's disease. Under the studied conditions (pH 3.1) Aβ large mass oligomers assemble into elongated amyloid fibrils via a diffusion–coalescence mechanism, which is controlled by a single activation barrier (Carrotta et al. 2005). Here, we extended the observations to the late stage of the aggregation process when larger aggregates are formed (Figs. 1, 2, 3).

Experiments have been performed with several scattering techniques: SALS, HNFS, LALS, USAXS, and SAXS. The usage of these methods allowed us to study the morphological properties of aggregates over several lengthscales from nanometers to tens of micrometers that is spanning five orders of magnitude.

The amyloid fibrils, formed after a few days of incubation, are rather cylindrical objects with an average diameter of 7.6 nm and a length of more than a hundred nanometers (Fig. 5). After a few months of incubation at 37°C, the fibrils are assembled into large size bundles (Fig. 3). Such bundles keep an elongated shape, which is likely given by their fibrillar constituents. They have a typical size of a few tens of micrometers and are obtained by a compact packing of objects with an average size of tens of nanometers (Fig. 4).

We have proposed a consistent explanation of the morphological properties of amyloid bundles of fibrils, by fitting the scattering data with a hierarchical form factor (Eqs. 2, 3, 5–7). This model allows one to understand the main structural features of amyloid bundles, by encompassing all the lengthscales involved, from the large bundles to their fibrillar constituent (Fig. 6). It would be of great interest to extend such study to other conditions and to compare these results with the in vivo observations of amyloid deposits, such as senile plaques or cerebral amyloid angiopathy.

Acknowledgments We thank D. Bulone, M. Di Carlo, D. Giacomazza, R. Noto for their collaboration and discussions.

References

Ban T, Hoshino M, Takahashi S, Hamada D, Hasegawa K, Naiki H, Goto Y (2004) Direct observation of Aβ amyloid fibril growth and inhibition. J Mol Biol 344:757–767

Berne BJ, Pecora R (1976) Dynamic light scattering. Wiley Interscience, New York

Borsboom M, Bras W, Cerjak I, Detollenaere D, Glastra van Loon D, Goedtkindt P, Konijnenburg M, Lassing P, Levine YK, Munneke B, Oversluizen M, van Tol R, Vlieg E (1998) The dutch–belgian beamline at the esrf. J Synchroton Rad 5:518–520

Bras W (1998) A saxs/waxs beamline at the esrf and future experiments. J Macromol Sci Phys B 37:557–566

Bulone D, Giacomazza D, Martorana V, Newman J, San Biagio PL (2004) Ordering of agarose near the macroscopic gelation point. Phys Rev E 69:0411401-1–0411401-9

Carrotta R, Manno M, Bulone D, Martorana V, San Biagio PL (2005) Protofibril formation of amyloid β-protein at low pH via a non-cooperative elongation mechanism. J Biol Chem 280:30001–30008

Carrotta R, Di Carlo M, Manno M, Montana G, Picone P, Romancino D, San Biagio PL (2006) Toxicity of recombinant β-amyloid prefibrillar oligomers on the morphogenesis of the sea urchin paracentrotus lividus. FASEB J 20:1916–1917

Ferri F, Magatti D, Pescini D, Potenza MAC, Giglio M (2004) Heterodyne near-field scattering: a technique for complex fluids. Phys Rev E 70:041405-1–041405-9

Georganopoulou DG, Chang L, Nam J-W, Thaxton CS, Mufson EJ, Klein WL, Mirkin CA (2005) Nanoparticle-based detection in cerebral spinal Fluid of a soluble pathogenic biomarker for Alzheimer's disease. Proc Natl Acad Sci (USA) 102:2273–2276

Glenner GG, Wong CW (1984) Alzheimer's disease: initial report of the purification and characterization of a novel cerebrovascular amyloid protein. Biochem Biophys Res Commun 120:885–890

Hammersley AP (1997) Fit2d: an introduction and overview. ESRF Internal Report ESRF97HA02T Hardy J, Selkoe DJ (2002) The amyloid hypothesis of Alzheimer's disease: Progress and problems on the road to therapeutics. Science 297:353–356

Harper JD, Wong SS, Lieber CM, Lansbury PTJ (1997) Observation of metastable Aβ amyloid protofibrils by atomic force microscopy. Chem Biol 4:119–125

Hoshi M, Sato M, Matsumoto S, Noguchi A, Yasutake K, Yoshida N, Sato K (2003) Spherical aggregates of b-amyloid (amylospheroid) show high neurotoxicity and activate tau protein kinase I/glycogen synthase kinase-3β. Proc Natl Acad Sci USA 100:6370–6375

Huang THJ, Yang DS, Plaskos NP, Go S, Yip CM, Fraser PE, Chakrabartty A (2000) Structural studies of soluble oligomers of the Alzheimer β-amyloid peptide. J Mol Biol 297:73–87

Iwatsubo T, Odaka A, Suzuki N, Mizusawa H, Nukina N, Ihara Y (1994) Visualization of Aβ 42(43) and Aβ 40 in senile plaques with end-specific Aβ monoclonals: evidence that an initially deposited species is Aβ 42(43). Neuron 13:45–53

Lambert MP, Barlow AK, Chromy BA, Edwards C, Freed R, Liosatos M, Morgan TE, Rozovsky I, Trommer B, Viola KL,Wals P, Zhang C, Finch CE, Krafft GA (1998) Diffusible, nonfibrillar ligands derived from Aβ1–42 are potent central nervous system neurotoxins. Proc Natl Acad Sci USA 95:6448–6453

Lansbury PTJ (1999) Evolution of amyloid: what normal protein folding may tell us about fibrillogenesis and disease. Proc Natl Acad Sci USA 96:3342–3344

Lashuel HA, Hartley D, Petre BM, Walz T, Lansbury PTJ (2002) Amyloid pores from pathogenic mutations. Nature 418:291–291

Lomakin A, Chung DS, Benedek GB, Kirschner DA, Teplow DB (1996) On the nucleation and growth of amyloid β-protein fibrils: Detection of nuclei and quantitation of rate constants. Proc Natl Acad Sci USA 93:1125–1129

Manno M, Craparo EF, Martorana V, Bulone D, San Biagio PL (2006) Kinetics of insulin aggregation: disentanglement of amyloid fibrillation from large-size cluster formation. Biophys J 90:4585–4591

Manno M, Craparo EF, Podest_a A, Bulone D, Carrotta R, Martorana V, Tiana G, San Biagio PL (2007) Kinetics of different processes in human insulin amyloid formation. J Mol Biol 366:258–274

Mathis CA, Klunk WE, Price JC, DeKosky ST (2005) Imaging technology for neurodegenerative diseases. Arch Neurol 62:196–200

Muller-Hill B, Beyreuther K (1989) Molecular biology of Alzheimer's disease. Ann Rev Biochem 58:287–307

Nicolai T, Durand D, Gimel J-C (1996) In: Light scattering: Principles, development. In: W Brown (eds) Scattering properties and modeling of aggregating and gelling systems. Clarendon Press, Oxford, pp 201–231

Pedersen JS (1993) Small-angle scattering from precipitates: analysis by use of a polydisperse hard-sphere model. Phys Rev B 47:657–665

Pedersen JS (1997) Analysis of small-angle scattering data from colloids and polymer solutions: modelling and least-squares fitting. Adv Colloid Interface Sci 70:171–210

Pitschke M, Prior R, Haupt M, Riesner D (1998) Detection of single amyloid b-protein aggregates in the cerebrospinal fluid of Alzheimer's patients by fluorescence correlation spectroscopy. Nat Med 4:832–834

Rensink AAM, de Waal RMW, Kremer B, Verbeek MM (2003) Pathology of cerebral amyloid angiopathy. Brain Res Rev 43:207–223

Selkoe DJ (1999) Translating cell biology into therapeutic advances in Alzheimer's disease. Nature 399:A23–A31

Selkoe DJ (2002) Alzheimer's disease is a synaptic failure. Science 298:789–791

Small GW, Kepe V, Ercoli LM, Siddarth P, Bookheimer SY, Miller KJ, Lavretsky H, Burggren AC, Cole GM, Vinters HV, Thompson PM, Huang SC, Satyamurthy N, Phelps ME, Barrio JR (2006) Pet of brain amyloid and tau in mild cognitive impairment. New Engl J Med 355:2652–2663

Stepanek P (1993) In: Dynamic light scattering: The method, some application. In: Brown W (eds) Ch. Data analysis in dynamic light scattering. Clarendon Press, Oxford, pp 177–240

Temussi PA, Masino L, Pastore A (2003) From Alzheimer to Huntington: why is a structural understanding so difficult? EMBO J 22:355–361

Terry RD, Masliah E, Salmon DP, Butters N, DeTeresa R, Hill R, Hansen LA, Katzman R (1991) Physical basis of cognitive alterations in Alzheimer disease: synapse loss is the major correlate of cognitive impairment. Ann Neurol 30:572–580

Walsh DM, Lomakin A, Benedek GB, Condron MM, Teplow DB (1997) Amyloid β-protein fibrillogenesis: detection of a protofibrillar intermediate. J Biol Chem 272:22364–22372

Walsh DM, Klyubin I, Fadeeva JV, Cullen WK, Anwyl R, Wolfe MS, Rowan MJ, Selkoe DJ (2002) Naturally secreted oligomers of amyloid β protein potently inhibit hippocampal long-term potentiation in vivo. Nature 416:535–539

Westlind-Danielsson A, Arnerup G (2001) Spontaneous in vitro formation of supramolecular β-amyloid structures, ''βamy balls'', by β-amyloid 1–40 peptide. Biochemistry 40:14736–14743

Yong W, Lomakin A, Kirkitadze MD, Teplow DB, Chen S-H, Benedek GB (2002) Structure determination of micelle-like intermediates in amyloid β-protein fibril assembly using small angle neutron scattering. Proc Natl Acad Sci USA 99:150–154